Linear Polymers for Nonlinear Optics. 2. Synthesis and Electrooptical Properties of Polymers Bearing Pendant Chromophores with Methylsulfonyl Electron-Acceptor Groups[1]

Douglas R. Robello,* Phat T. Dao, James Phelan, Joseph Revelli, Jay S. Schildkraut, Michael Scozzafava, Abraham Ulman, and Craig S. Willand

Corporate Research Laboratories, Eastman Kodak Company, Rochester, New York 14650

Received October 9, 1991. Revised Manuscript Received January 16, 1992

Several acrylic polymers bearing pendant stilbene or azobenzene chromophores containing 4'-dialkylamino electron donors and 4-methylsulfonyl electron acceptors have been synthesized. These amorphous polymers exhibited good film-forming abilities, moderately high glass transition temperatures, and excellent optical clarity. Film samples of the polymers were poled in electric fields and demonstrated large, stable second-order nonlinear optical properties. Electrooptic coefficients at 632 nm were measured using ellipsometry. To demonstrate their utility in electrooptical devices, the title polymers were fabricated into low-loss waveguides, and Mach-Zehnder interferometers were constructed. Electrooptic coefficients as high as 12 pm/V were measured at 860 nm with these prototypical devices. Comparisons between experimental and predicted electrooptic coefficients are presented.

Introduction

Worldwide attention has been drawn to nonlinear optical (NLO) materials in recent years because of their potential to serve as the active components of ultrafast and highly efficient devices for optical communications, information processing, and computing.[2-7] *Organic* NLO materials, in particular, are thought to possess many potential advantages over existing inorganic materials, for example, as follows:

Processing. Many proposed optical devices require thin (ca. 1 μm) layers of NLO material on some substrate to act as waveguides. Although such structures have been formed by diffusing thin layers of titanium into single crystals of $LiNbO_3$ (a widely used inorganic NLO material), this process requires very high temperatures, and the crystals of $LiNbO_3$ are themselves quite expensive. In contrast, thin films of organic polymers can be formed by spin or dip coating from solution, and low molecular weight organic compounds can be vacuum evaporated onto a substrate. Additionally, complicated structures such as channels and junctions might be fabricated using conventional microlithography. These simple low-temperature processing methods would be compatible with existing silicon or gallium arsenide fabrication technology. Thus, it may be possible to integrate electronic and optical components on a single chip.

NLO Response. NLO processes in inorganic solids depend on contributions from distortion of the crystal lattice (phonons). In contrast, the NLO susceptibility in certain organic NLO materials is based entirely on virtual electronic transitions, which are inherently much faster processes (subfemtosecond time scale) than those involving phonons. Stated in a different way, the frequency range of organic NLO devices can potentially extend to many gigahertz without a significant falloff in susceptibility. In addition, organic materials have the potential for larger NLO properties than inorganics, although there have been few reports in which this advantage has been clearly demonstrated without resonance enhancement. Resonance enhancement occurs when the material absorbs some of the propagating light, leading to a stronger interaction and an apparent increase in NLO properties when measured in typical laboratory tests such as harmonic generation. However, the optical power density in most practical NLO waveguide devices is quite large; therefore, even small absorptions can cause intolerable damage to the material.

Device Characteristics. Most organic materials possess relatively low dielectric constants when compared to inorganic materials, a feature that also contributes to their potentially faster response times. In addition, if absorption losses can be minimized, organics should exhibit improved resistance to laser damage during device operation compared with inorganic materials.

The theoretical basis of optical nonlinearity in organics has been set forth;[2,4-9] nevertheless the processes for achieving large NLO effects in organic materials are not yet perfected. Also, the design of practical NLO materials is complicated by the need to simultaneously optimize many properties in addition to optical nonlinearity. These include electrical behavior, mechanical properties, thermal stability, processing methods, and linear optical properties such as refractive index and absorption characteristics.

Researchers have been seeking to exploit the second-order NLO susceptibility ($\chi^{(2)}$) for applications involving electrooptic modulation and switching, as well as frequency combination. (The well-known process of second harmonic generation (SHG) is a special case of frequency combination.) Because $\chi^{(2)}$ effects in organic materials arise fairly directly from the constituent molecules (rather than from

* To whom correspondence should be sent.

(1) Part 1: Robello, D. R. *J. Polym. Sci., Polym. Chem. Ed.* **1990**, *28*, 1.
(2) Williams, D. J. *Angew. Chem., Int. Ed. Engl.* **1984**, *23*, 690-703.
(3) Williams, D. J., Ed. *Nonlinear Optical Properties of Organic and Polymeric Materials*; ACS Symposium Series 233; American Chemical Society: Washington, DC, 1983.
(4) Chemla, D. S.; Zyss, J. *Nonlinear Optical Properties of Organic Molecules and Crystals*; Academic Press: New York, 1987.
(5) Williams, D. J. In *Electronic and Photonic Applications of Polymers*; Bowden, M. J., Turner, S. R., Eds.; Advances in Chemistry 218; American Chemical Society: Washington, DC, 1989; pp 297-330.
(6) Prasad, P. N.; Williams, D. J. *Introduction to Nonlinear Optical Effects in Molecules and Polymers*; Wiley: New York, 1991.
(7) Marder, S. R.; Sohn, J. E.; Stucky, G. D. *Materials for Nonlinear Optics*; ACS Symposium Series 455; American Chemical Society: Washington, DC, 1991.
(8) Meredith, G. R.; VanDusen, J. G.; Williams, D. J. *Macromolecules* **1984**, *17*, 2228-2230.
(9) Singer, K. D.; Kuzyk, M. G.; Sohn, J. E. *J. Opt. Soc. Am. B* **1987**, *4*, 968-976.

0897-4756/92/2804-0425$03.00/0

some bulk property, as, for example, in semiconductors), it is possible to predict $\chi^{(2)}$ with reasonable accuracy based only on the molecular structure and the processing conditions (and the crystal structure, if applicable). In this paper, we complete a logical progression from theory to molecules to materials to devices. Our previous work involving molecular theoretical calculations and measurements[10] has been extended to the synthesis and characterization of polymeric materials, and the construction of prototypical NLO devices. We have exploited the oftencited ability of organic materials be to fine-tuned by synthesis to achieve the required balance of properties. In this way, large stable second-order NLO susceptibilities were combined with excellent optical transparency, film integrity, and other desirable physical properties. We also demonstrate the accuracy of $\chi^{(2)}$ predictions, particularly in cases for which the dispersion correction to β is small.

It is well-known that organic molecules containing electron donating and accepting groups separated by a conjugated π-framework exhibit large molecular hyperpolarizabilities (β). While much of the published work in second-order nonlinear optics deals with compounds containing nitro[1,8,9,11-23] and cyanovinyl[24-32] acceptors, we have recently shown that sulfonyl groups[10,33,34] are attractive alternatives because they cause a desirable (relative) blue-shift in absorbance, at the cost of only a modest decrease in β. In addition, the available valence on the sulfonyl group provides synthetic flexibility for fine-tuning the physical properties of the material or for the creation of novel chromophore-containing compounds.[35-38]

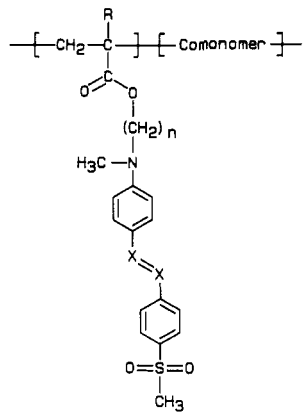

NLO Polymer	R	n	X	Comonomer
1	CH_3	2	N	none
2	CH_3	6	N	none
3	CH_3	6	N	methyl methacrylate
4	H	6	CH	4-t-butylstyrene
5	H	6	CH	methyl methacrylate

Figure 1. NLO polymer structures.

Because of symmetry considerations, materials containing a center of inversion (including amorphous materials) exhibit no second-order NLO properties. One method of achieving noncentrosymmetry is by electric field poling, which has begun to be studied by a number of groups.[8-14,18,19,26,27,29,39] In this technique, NLO-active molecules in a *mobile* state are aligned in a strong dc electric field, and the induced orientation is fixed by solidifying the material using either cooling or chemical reaction. A number of early studies involved the poling of guest compounds dispersed in a host matrix;[8,9,11,14,39] however, it was quickly recognized that covalent attachment of the NLO-active chromophores to the matrix not only provided higher chromophore densities but also improved the long-term stability of alignment.[12] Much research has focused on liquid-crystalline materials for second-order nonlinear optics[1,8,15,16,18,19] due to their inherently high order. However, scattering caused by disinclinations and grain boundaries in liquid-crystal materials reduces the light intensity within a waveguide and decreases the signal-to-noise ratio of the device.

As part of a program to develop integrated optical devices based on organic materials, we have initiated a study of the NLO properties of some amorphous organic polymers that contain covalently bound chromophores with methylsulfonyl acceptor groups (Figure 1). The chromophores are attached to acrylic backbones via flexible spacer groups, which allowed for rapid electric field poling near the glass transition temperatures of the polymers. After cooling the polymers to room temperature and removal of the poling field, we measured the second-order nonlinear optical susceptibility of the materials using el-

(10) Ulman, A.; Willand, C. S.; Köhler, W.; Robello, D. R.; Williams, D. J.; Handley, L., *J. Am. Chem. Soc.* **1990**, *112*, 7083-7090.
(11) Singer, K. D.; Sohn, J. E.; Lalama, S. J. *Appl. Phys. Lett.* **1986**, *49*, 248-250.
(12) Singer, K. D.; Kuzyk, M. G.; Holland, W. R.; Sohn, J. E.; Lalama, S. J.; Comizzoli, R. B.; Katz, H. E.; Schilling, M. L. *Appl. Phys. Lett.* **1988**, *53*, 1800-1802.
(13) Hill, J. R.; Pantelis, P.; Abbasi, F.; Hodge, P. *J. Appl. Phys.* **1988**, *64*, 2749-2751.
(14) Hampsch, H. L.; Yang, J.; Wong, G. K.; Torkelson, J. M. *Macromolecules* **1988**, *12*, 526-528; *Polym. Commun.* **1989**, *30*, 40.
(15) Griffin, A. C.; Bhatti, A. M.; Hung, S. L. *Proc. SPIE*, **1987**, *682*, 65.
(16) LeBarney, P.; Ravaux, G.; Dubois, J. C.; Parneix, J. P.; Njeumo, R.; Legrand, C.; Levelut, A. M. *Proc. SPIE* **1987**, *682*, 56.
(17) Matsumoto, S.; Kubodera, K.; Kurihara, T.; Kaino, T. *Appl. Phys. Lett.* **1987**, *51* (*1*), 1.
(18) Buckley, A.; Choe, E.; DeMartino, R.; Leslie, T.; Nelson, G.; Stamatoff, J.; Stuetz, D.; Yoon, H. *Polym. Mater. Sci. Eng.* **1986**, *54*, 502.
(19) DeMartino, R.; Haas, D.; Khanarian, G.; Leslie, T.; Man, H. T.; Riggs, J.; Sansone, M.; Stamatoff, J.; Teng, C.; Yoon, H. *Mater. Res. Soc. Symp. Proc.* **1988**, *109*, 65-76.
(20) DeMartino, R. N.; Yoon, H.-N.; Stamatoff, J. B.; Buckley, A. U.S. Patent 4,694,066, 1987.
(21) DeMartino, R. N. U.S. Patent 4,717,508, 1988; 4,757,130, 1988; 4,779,961, 1988.
(22) DeMartino, R. N.; Yoon, H.-N. U.S. Patent 4,801,670, 1989; 4,808,332, 1989; 4,822,865, 1989; 4,865,430, 1989.
(23) Leslie, T. M. U.S. Patent 4,807,968, 1989; 4,855,078, 1989.
(24) Choe, E. W. U.S. Patent 4,603,187, 1986; 4,755,574, 1988.
(25) Eich, M.; Sen, A.; Looser, H.; Bjorklund, G. C.; Swalen, J. D.; Twieg, R.; Yoon, D. Y. *J. Appl. Phys.* **1989**, *66*, 2559-2567.
(26) Eich, M.; Reck, B.; Yoon, D. Y.; Wilson, C. G.; Bjorklund, G. C. *J. Appl. Phys.* **1989**, *66*, 3241-3247.
(27) Hubbard, M. A.; Marks, T. J.; Yang, J.; Wong, G. K. *Chem. Mater.* **1989**, *1*, 167-169.
(28) Katz, H. E.; Singer, K. D.; Sohn, J. E.; Dirk, C. W.; King, L. A.; Gordon, H. M. *J. Am. Chem. Soc.* **1987**, *108*, 6561-6563.
(29) Katz, H. E.; Dirk, C. W.; Singer, K. D.; Sohn, J. E. *Mol. Cryst. Liq. Cryst.* **1988**, *157*, 525-533.
(30) Choe, E. W.; Buckley, A.; Garito, A. F. U.S. Patent 4,640,800, 1987; 4,667,042, 1987; 4,707,305, 1987; 4,773,743, 1988; 4,774,025, 1988.
(31) Choe, E. W. U.S. Patent 4,694,048, 1987.
(32) Choe, E. W.; Khanarian, G.; Garito, A. F. U.S. Patent 4,732,783, 1988.
(33) Ulman, A.; Williams, D. J.; Penner, T. L.; Robello, D. R.; Schildkraut, J. S.; Scozzafava, M.; Willand, C. S. U.S. Patent 4,792,208, 1988.
(34) Nijhuis, S.; Rikken, G. L. J. A.; Havinga, E. E.; tenHoeve, W.; Wynberg, H.; Meijer, E. W. *J. Chem. Soc., Chem. Commun.* **1990**, 1093.
(35) Robello, D. R.; Schildkraut, J. S.; Armstrong, N. J.; Penner, T. L.; Köhler, W.; Willand, C. S. *Polym. Prepr. (Am. Chem. Soc., Div. Polym. Chem.)* **1991**, *32* (*3*), 78-79.
(36) Penner, T. L.; Willand, C. S.; Robello, D. R.; Schildkraut, J. S.; Ulman, A. *Proc. SPIE* **1991**, *1436*, 169.
(37) Köhler, W.; Robello, D. R.; Willand, C. S.; Williams, D. J. *Macromolecules* **1991**, *24*, 4589-99.
(38) Köhler, W.; Robello, D. R.; Dao, P. T.; Willand, C. S.; Williams, D. J. *J. Chem. Phys.* **1990**, *93*, 9157.
(39) Williams, D. J., in ref 4, pp 405-435.

lipsometry.[40,41] Finally, to investigate the utility of these materials under conditions more closely simulating those found in a realistic electrooptic device, we constructed Mach–Zehnder interferometers using two of the title polymers. In this way, the electrooptic coefficients were measured in the near-infrared, an important wavelength region for optical devices.

Experimental Section

Materials. NMR spectra were obtained on a General Electric QE-300 spectrometer, operating at 300 MHz for ^1H and 75.5 MHz for ^{13}C. Elemental analyses, differential scanning calorimetry (DSC), size exclusion chromatography (SEC), and field desorption mass spectroscopy (FD-MS) were performed by Eastman Kodak Co., Analytical Technology Division.

N-(2-Hydroxyethyl)-*N*-methylaniline (**6**, Pfaltz and Bauer Research Chemicals) was distilled before use, bp 90–104 °C (0.04 mmHg). *N*-(6-Hydroxyhexyl)-*N*-methylaniline[1] (**7**), 4-[(6-acetoxyhexyl)methylamino]benzaldehyde[1] (**8**), 4-(methylsulfonyl)-aniline[10] (**9**), and diethyl 4-(methylsulfonyl)benzylphosphonate[10] (**10**) were prepared by published procedures.

4′-[(2-Hydroxyethyl)methylamino]-4-(methylsulfonyl)-azobenzene (11). A suspension of 20.0 g (0.117 mol) of 4-(methylsulfonyl)aniline (**9**) in 150 mL of 50% aqueous HCl at 0 °C was treated dropwise with 10.9 g (0.128 mol) of sodium nitrite dissolved in 30 mL of water. *N*-(2-Hydroxyethyl)aniline (**6**, 19.4 g, 0.128 mol) was added slowly, the resulting mixture was stirred for 15 min at 0 °C, and then 15 g of sodium acetate was added. The reaction mixture was stirred 2 h at 0 °C and 16 h at 23 °C. The precipitated product was filtered and washed successively with water, 10% aqueous acetic acid, and again with water. The brown solid was air dried, and recrystallized from ethanol/pyridine and then from toluene/tetrahydrofuran. A red powder was obtained, mass 11.9 g (30%). A small amount (2.2 g) of less-pure product was obtained by concentration of the mother liquors followed by flash chromatography (silica gel, 20% ether/80% dichloromethane).

^1H NMR ($(CD_3)_2SO$) δ 3.09 (s, 3 H), 3.26 (s, 3 H), 3.6 (m, 4 H), 4.80 (t, J = 5.1, 1 H), 6.86 (d, J = 9.2, 2 H), 7.81 (d, J = 9.1, 2 H), 7.99 (AB, $\Delta\nu$ = 31.7, J = 8.6, 4 H). All J values are in hertz. $^{13}C\{^1H\}$ NMR ($(CD_3)SO$) δ 43.6, 54.0, 58.2, 79.1, 111.5, 122.2, 125.6, 128.3, 140.2, 142.4, 152.6, 155.3.

4′-[(6-Hydroxyhexyl)methylamino]-4-(methylsulfonyl)-azobenzene (12). A stirred suspension of 150 g (0.88 mol) of 4-(methylsulfonyl)aniline (**9**) in 1 L of 20% hydrochloric acid at 0–3 °C was treated dropwise with a solution of 66.5 g (0.96 mol) of sodium nitrite in 200 mL of water. *N*-(6-Hydroxyhexyl)-*N*-methylaniline (**7**, 218 g, 1.05 mol) was added slowly, maintaining the temperature below 5 °C, and the mixture was stirred for 1 h. Sodium acetate (119 g, 0.88 mol) was added, and stirring was continued for 3 h. Concentrated ammonium hydroxide (250 mL) was added slowly, and the mixture was stirred for 64 h. The precipitated product was filtered, air dried, and recrystallized successively from ethanol, from toluene, and then from toluene/isopropyl alcohol to produce 160 g (47%) of a red solid, mp 114–116 °C.

^1H NMR ($CDCl_3$) δ 1.4 (m, 4 H), 1.6 (m, 4 H), 3.07 (s, 3 H), 3.08 (s, 3 H), 3.43 (t, J = 7.5, 2 H), 3.64 (t, J = 6.4, 2 H), 6.72 (d, J = 9.2, 2 H), 7.88 (d, J = 9.1, 2 H), 7.98 (AB, J = 8.7, $\Delta\nu$ = 20.3, 4 H). $^{13}C\{^1H\}$ NMR ($CDCl_3$) δ 25.7, 26.8, 27.1, 38.7, 44.6, 52.6, 62.7, 111.3, 122.7, 126.0, 128.4, 139.7, 143.4, 152.4, 156.5.

4′-[(2-(Methacroyloxy)ethyl)methylamino]-4-(methylsulfonyl)azobenzene (13). A solution of 12.5 g (37.5 mmol) of 4′-[(2-hydroxyethyl)methylamino]-4-(methylsulfonyl)azobenzene (**11**), 4.6 g (45 mmol) of triethylamine, and ca. 50 mg of 3-*tert*-butyl-4-hydroxy-5-methylphenyl sulfide (inhibitor) in 100 mL of dry tetrahydrofuran at 0 °C was treated dropwise with 4.7 g (45 mmol) of freshly distilled methacryloyl chloride. The reaction mixture was stirred for 1 h at 0 °C and for 18 h at 25 °C and then washed with brine, saturated aqueous $NaHCO_3$, and brine. The solution was dried ($MgSO_4$) and was concentrated at reduced pressure. TLC of the solid residue indicated that some unreacted **11** was present, so the solid was redissolved in 150 mL of dry dichloromethane and reacted with an additional 3 g of methacryloyl chloride and 3 g of triethylamine for 24 h at 23 °C. The resulting solution was washed successively with water, saturated aqueous $NaHCO_3$, and water. The organic layer was dried ($MgSO_4$), and the solvent was removed at reduced pressure to deposit a red solid that was recrystallized from tetrahydrofuran/hexanes to produce 8.8 g (58%) of orange plates.

^1H NMR ($CDCl_3$) δ 1.91 (s, 3 H), 3.09 (s, 3 H), 3.14 (s, 3 H), 3.80 (t, J = 5.7, 2 H), 4.38 (t, J = 5.7, 2 H), 5.67 (s, 1 H), 6.07 (s, 1 H), 6.80 (d, J = 9.1, 2 H), 7.89 (d, J = 9.0, 2 H), 8.01 (AB, $\Delta\nu$ = 19.3, J = 8.6, 4 H). $^{13}C\{^1H\}$ NMR ($CDCl_3$) δ 18.3, 39.0, 44.6, 50.8, 61.7, 111.5, 122.8, 125.9, 126.2, 128.4, 135.8, 139.8, 143.8, 152.1, 156.2, 167.2. FD-MS 401 m/e (M^+).

4′-[(6-(Methacroyloxy)hexyl)methylamino]-4-(methylsulfonyl)azobenzene (14). A mixture of 141 g (0.362 mol) of 4′-[(6-hydroxyhexyl)methylamino]-4-(methylsulfonyl)azobenzene (**12**), 37.0 g (0.366 mol) of triethylamine, 400 mg of 3-*tert*-butyl-4-hydroxy-5-methylphenyl sulfide (inhibitor), and 500 mL of dry dichloromethane was treated with methacryloyl chloride (52.7 g, 0.504 mol) at 0 °C under nitrogen. The reaction mixture was stirred for 1 h at 0 °C and then for 12 h at 23 °C. The reaction mixture was washed with 500 mL of water to remove precipitated triethylamine hydrochloride, then with 500 mL of saturated $NaHCO_3$, and finally with 500 mL of water. The organic layer was dried (Na_2SO_4), and the solvent was removed at reduced pressure to deposit a dark orange oil that crystallized on trituration with hexanes. The product was recrystallized from toluene and then from THF/hexanes to provide 124 g (75%) of orange powder, mp 78–80 °C.

^1H NMR ($CDCl_3$) δ 1.44 (m, 4 H), 1.69 (m, 4 H), 1.95 (s, 3 H), 3.09 (s, 6 H), 3.45 (t, J = 7.4, 2 H), 4.16 (t, J = 6.6, 2 H), 5.56 (s, 1 H), 6.10 (s, 1 H), 6.74 (d, J = 9.2, 2 H), 7.90 (d, J = 9.1, 2 H), 8.00 (AB, J = 8.7, $\Delta\nu$ = 19.8, 4 H). $^{13}C\{^1H\}$ NMR ($CDCl_3$) δ 18.3, 25.9, 26.7, 27.0, 28.6, 38.7, 44.6, 52.5, 64.5, 111.3, 122.7, 125.1, 126.0, 128.3, 136.5, 139.8, 143.5, 152.4, 156.4, 167.4. FD-MS 457 (M^+). Anal. Calcd for $C_{24}H_{31}N_3O_4S$: C, 63.00; H, 6.83; N, 9.12; S, 7.01. Found: C, 62.96; H, 6.56; N, 9.12; S, 7.83.

4′-[(6-Hydroxyhexyl)methylamino]-4-(methylsulfonyl)-stilbene (15). To a solution of 5 g (0.125 mol) of 60% sodium hydride dispersion, 27.7 g (0.1 mol) of 4-[(6-acetoxyhexyl)-methylamino]benzaldehyde (**8**), and 200 mL of dry, freshly distilled 1,2-dimethoxyethane (DME) under nitrogen, at room temperature, with vigorous stirring was added 30.6 g (0.1 mol) of diethyl 4-(methylsulfonyl)benzylphosphonate (**10**). The mixture immediately turned yellow. The reaction mixture was heated at reflux for 2 h. The bright yellow solution was poured over 400 g of crushed ice under nitrogen, and the resulting mixture was extracted with four 250-mL portions of dichloromethane. The combined organic extracts were washed three times with 250 mL of water, and the solvent was removed at reduced pressure. The residue was dissolved in 250 mL of 10% (v/v) HCl in 1:1 ethanol:water, and the solution was heated at reflux for 4 h. After cooling, the solution was neutralized to pH 7 by the slow and careful addition of sodium carbonate. The yellow solid thus formed was collected by filtration, washed with water, and air dried. Recrystallization from methanol yielded 31.4 g (81%) of a bright yellow solid. This material contained some acetate that was not hydrolyzed ($\simeq$5%); however, a pure sample of the material was obtained by chromatography. Thus, 5 g of the material was dissolved in 25 mL of a mixture of acetone:ethyl acetate 1:5 and loaded onto a dry silica gel column (500 g, 2-in. diameter). Elution gave 4.5 g of product that was then recrystallized from absolute methanol, mp 113–115 °C.

^1H NMR ($CDCl_3$) δ 1.45 (m, 4 H), 1.63 (m, 4 H), 3.01 (s, 3 H), 3.09 (s, 3 H), 3.39 (t, 2 H), 3.69 (br t, 2 H), 6.67 (d, J = 8.7, 2 H), 6.89 (d, J = 16.2, 1 H), 7.18 (d, J = 16.2, 1 H), 7.41 (d, J = 8.7, 2 H), 7.60 (d, J = 8.3, 2 H), 7.87 (d, J = 8.4, 2 H).

4′-[(6-(Acryloyloxy)hexyl)methylamino]-4-(methylsulfonyl)stilbene (16). A stirred mixture of 4′-[(6-hydroxyhexyl)methylamino]-4-(methylsulfonyl)stilbene (**15**, 20.0 g, 52 mmol), triethylamine (6.3 g, 62 mmol), and dry dichloromethane (DCM) was treated dropwise with acryloyl chloride (5.6 g, 62 mmol) in 50 mL of DCM at 23 °C under nitrogen. The resulting solution was stirred at 23 °C for 72 h and then filtered. The filtrate

(40) Schildkraut, J. *Appl. Opt.* **1988**, *27*, 329.
(41) Teng, C. C.; Man, H. T. *Appl. Phys. Lett.* **1990**, *56*, 1734–1736.

was washed successively with saturated NaCl, with saturated $NaHCO_3$, and with water. The organic layer was dried ($MgSO_4$), and the solvent was removed at reduced pressure to deposit a yellow oil that gradually crystallized. The product was recrystallized from tetrahydrofuran (THF)/hexanes to yield 15.5 g (68%) of a yellow solid, mp 88–90 °C.

^1H NMR ($CDCl_3$) δ 1.40 (m, 4 H), 1.70 (m, 4 H), 3.00 (s, 3 H), 3.06 (s, 3 H), 3.37 (t, 2 H), 4.17 (t, 2 H), 5.82 (dd, 1 H), 6.12 (m, 1 H), 6.40 (dd, 1 H), 6.70 (d, 2 H), 6.91 (d, 1 H), 7.09 (d, 1 H), 7.44 (d, 1 H), 7.62 (d, 2 H), 7.88 (d, 2 H). $^{13}C\{^1H\}$ NMR ($CDCl_3$) δ 25.8, 26.7, 28.6, 44.6, 64.4, 121.4, 126.3, 127.2, 127.7, 128.3, 128.6, 129.5, 130.2, 130.4, 148.3. Anal. Calcd for $C_{25}H_{31}NO_4S$: C, 68.00; H, 7.08; N, 3.17; S, 7.26. Found: C, 68.01; H, 6.86; N, 2.98; S, 6.89.

Note: The above procedure was repeated using methacryloyl chloride in place of acryloyl chloride, but the oily product (17) polymerized spontaneously after purification by flash chromatography and removal of solvent at reduced pressure. This polymer was insoluble in all solvents tried.

Polymerization Procedure. The following description of the polymerization of 4′-[(6-methacroyloxy)hexyl)methylamino]-4-(methylsulfonyl)azobenzene (14) is typical of the procedures used to synthesize polymers 1–5. Synthetic results and characterization data are summarized in Tables I and II, respectively.

Nitrogen gas was bubbled through a solution of 156 g (0.431 mol) of 14 and 0.64 g (0.0039 mol) of 2,2-azobis(2-methylpropionitrile) in 700 mL of *N,N*-dimethylformamide (DMF) for 15 min at 23 °C to remove dissolved oxygen. The solution was stirred at 60 ± 2 °C for 24 h and then cooled. The polymer was precipitated into excess methanol in a blender, and the resulting orange powder was filtered and washed with methanol. After air drying, the solid was redissolved in dichloromethane, the solution was filtered through a 20-μm filter, and the polymer was reprecipitated into agitated methanol. The polymer was reprecipitated once more from DMF into agitated deionized water, and the resulting powder was filtered, washed with water, and dried in a vacuum oven at 80 °C to constant mass.

Polymer Film Spin Coating. Polymer was dissolved in 1,2,3-trichloropropane (distilled from CaH_2 and passed through a basic Al_2O_3 column) at a concentration of between 10 and 20 wt % depending on the desired film thickness. The solution was applied to the substrate with a glass syringe through a filter (Millipore, 0.22 μm Millex-GS) until the substrate was completely covered. The substrate was then spun at 500 rpm for 5 s followed by 2000 rpm for 60 s. After coating, the films were heated to 120 °C at 0.025 mmHg for about 15 h to remove residual solvent.

Index of Refraction, Thickness, and Optical Density. The index of refraction, n, at 632.8 nm and thickness, d, of the polymer films were measured by determining the propagation constants of at least the two lowest order transverse electric optical guided modes for samples cast on fused silica substrates. The modes were excited by a HeNe laser beam that was prism coupled into the film. Using the propagation constants, the mode equation for a three-layer waveguide was solved for n and d.

The absorption spectrum of the film used in the waveguide experiment was determined at visible wavelengths. This provided the optical density (OD) per unit of thickness, which was used subsequently to calculate the thickness of a film on a transparent substrate from an OD measurement.

Dielectric Constant. A polymer film was coated on indium tin oxide (ITO) covered glass. Subsequently, circular gold electrodes (3-mm diameter) were evaporated on the film. The capacitance of the gold–polymer–ITO structure was determined with a HP 4192A LF impedance analyzer set at 1 kHz and 1 V rms. The thickness of the polymer film was determined by measuring its visible absorption and using the OD/d value as discussed above. Using electrode area A, capacitance C, and thickness d, the dielectric constant ϵ was calculated using the relationship $\epsilon = dC/A\epsilon_0$, where ϵ_0 is the electric permittivity of free space.

Poling. Polymer films for poling were prepared in the same way as those for dielectric constant measurements. To align the chromophores, a film was slowly heated to near its T_g and then a positive voltage was applied to the gold electrode. The ITO electrode was grounded. After 1 h, the heater was turned off and the film was allowed to cool below 30 °C, at which point the voltage was turned off. Typical cooling time was about 1 h.

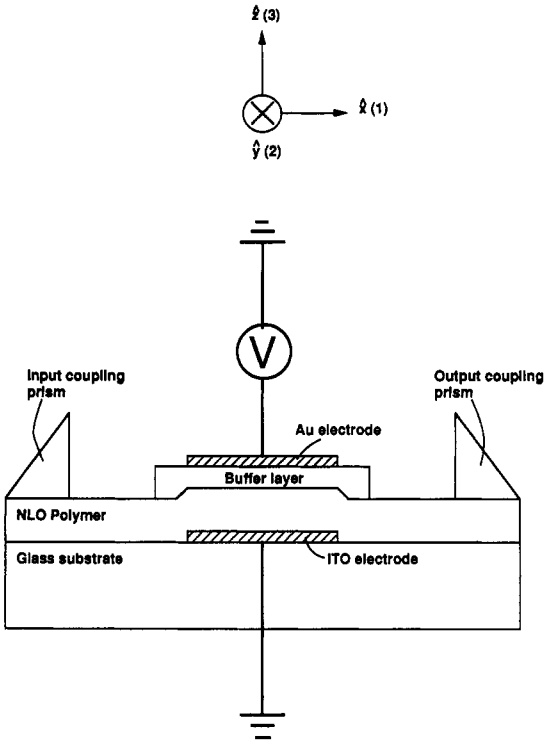

Figure 2. Cross-sectional schematic of waveguide used for Mach–Zehnder interferometry.

Corona poling was done using an apparatus consisting of a discharge source provided by three tungsten wires housed in a grounded anodized aluminum shell, and a stainless steel grid that served as the sample voltage controller. The corona wires were connected to a high-voltage power supply (Trek, Model 610C), operating typically at 5–7 kV. A second Trek power supply was used to charge the grid to a few hundered volts. The samples were heated in dry air atmosphere to near their glass transition temperatures, and then the corona discharge was applied for 30 min. The samples were cooled at 2 °C/h to ambient with the field still applied. Surface potentials were measured using an electrostatic voltmeter probe (Trek, Model 344).

Electrooptic Measurements. The electrooptic effect was observed using an ellipsometer (Gaertner, Model L116B) to measure the relative amplitude and phase change of reflected light of p and s polarization. The relative phase shift, Δ, of a 632.8-nm HeNe laser beam passed through the glass, ITO, and polymer film, and reflected from the gold electrode was measured as a function of applied voltage.[40,41]

Waveguide Fabrication. Figure 2 shows a cross-sectional view of the waveguide structure, and Table V lists the thicknesses and indexes of the various layers. The 50 × 50 × 1 mm soda lime glass substrate was initially prepared by rf sputter coating a 10-mm-wide stripe of thin transparent ITO across the center of the plate. The thin ITO stripe was processed in such a way to minimize optical loss for light propagating in the adjacent NLO waveguide layer while maintaining reasonable electrical conductivity. The NLO polymer was then spin coated on the glass substrate as described previously. A small, out-of-the-way patch of the NLO film was removed by rubbing with a cotton swab dipped in acetone so that electrical contact could be made to the ITO stripe. A contact wire was attached to the ITO film with silver-loaded epoxy. After grounding the ITO electrode, the NLO polymer film was then corona-poled[12] (see above) at a temperature just below the glass transition (see Table VI) and was cooled slowly to room temperature with the corona field applied. The indane derivative monomer glass (structure shown in Figure 5) was then evaporated through a 15 × 15 mm mask placed directly over the center of the ITO stripe to form the upper cladding/buffer layer. Finally, a 500-Å-thick Au upper electrode was evaporated through a mask centered on the monomer glass buffer. The Au pad was made small enough to fit within the area of the monomer buffer. Electric fields were applied to the region defined by the upper Au and

Scheme I. Synthesis of Donor Portion of NLO Monomers

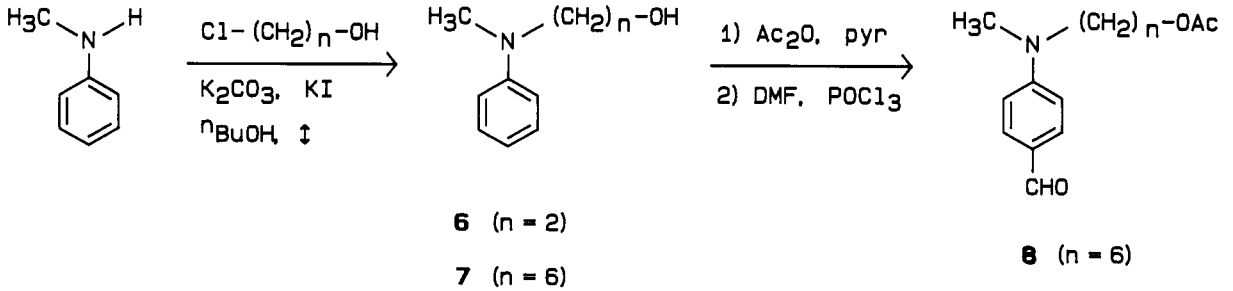

6 (n = 2)

7 (n = 6)

8 (n = 6)

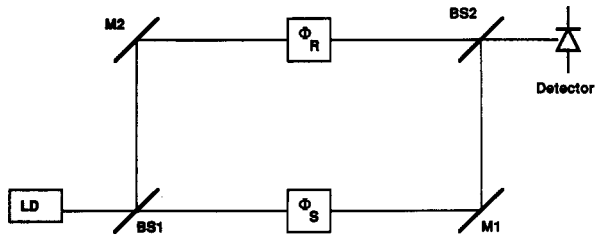

Figure 3. Schematic of Mach–Zehnder interferometer.

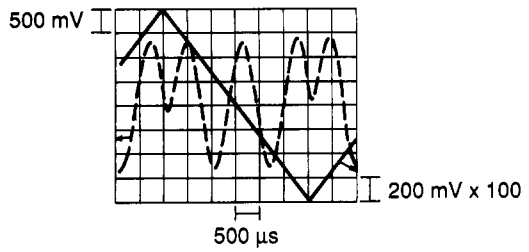

Figure 4. Typical oscilloscope trace for Mach–Zehnder experiment.

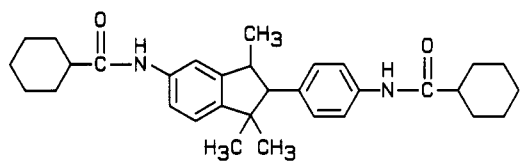

Figure 5. Indane derivative used as buffer layer.

lower ITO electrodes by putting a voltage source across these electrodes. Light was coupled into and out of the NLO waveguides using glass prisms (n_p = 1.864 at λ = 830 nm) with the light propagating in a direction perpendicular to the ITO stripe and passing beneath the Au electrode. The dimension of the Au electrode along the propagation direction defined the path length L (see eq 15 and Table V).

Optical losses in the waveguides were measured by imaging the streak produced in samples fabricated similarly to those in the previous paragraph, but without the upper gold electrode.

Mach–Zehnder Measurements. Figure 6 shows a detailed view of the Mach–Zehnder experimental arrangement. Light from an infrared laser diode was collimated with lens L1, and the polarization was adjusted to be either TE or TM by means of half-wave plate HWP in combination with Glan–Taylor polarizer P. Beamsplitter BS1 split the beam into sample and reference beams. The sample beam was weakly focused by lens L2 (f = 400 mm) onto the base of the input coupling prism. The NLO waveguide and prism assembly was mounted on a rotary stage so that light could be coupled selectively into specific modes of the NLO waveguide by adjusting the incidence angle. Light was coupled out of the NLO waveguide and directed by mirror M1 to a spatial filter/recollimator formed by lenses L3 and L4 and pinhole H. The spatial filter removes wavefront aberrations introduced by propagation of the light through the NLO waveguide. The reference beam was directed through variable attenuator A which was adjusted to equalize the intensities of the sample and reference beams at the photodetector PD. Mirrors M2, M3, and M4 permitted adjustment of the optical pathlength of the reference beam to match that of the sample beam to within the coherence length of the light from the laser diode. The reference and sample beams were then recombined at beamsplitter BS2, and the two resulting interferograms were directed toward a CCD camera and a silicon photodiode, respectively. The CCD camera permitted observation of the interferogram during data taking. A function generator (HP Type 8116A) was used to generate 100–200-Hz triangle-shaped wave forms which were subsequently amplified by a high-voltage operational amplifier (Burleigh Model PZ-70). The function generator also provided the trigger pulse to begin the oscilloscope trace. The voltage applied to the sample was typically ramped linearly in time between 0 and 160 V. The outputs of both the photodetector PD and the high-voltage op amp were monitored with the oscilloscope. Note the 100× attenuator between the op amp and the oscilloscope. Figure 4 shows a typical oscilloscope trace showing the triangle input voltage waveform and the sinusoidal photodetector output.

Table I. Synthesis Data for NLO Polymers 1–5

polym	NLO monomer	comonomer[a]	mol % NLO monomer (feed/polym)[b]	solv[c]	yield, %
1	13	none	100/100	DMF	74
2	14	none	100/100	DMF	87
3	14	MMA	18/19	PhCl	94
4	16	TBS	11/11	PhCl	50
5	16	MMA	8/7	PhCl	80

[a] MMA = methyl methacrylate; TBS = 4-*tert*-butylstyrene. [b] Composition of polymers determined by ^{1}H NMR. [c] DMF = *N*,*N*-dimethylformamide; PhCl = chlorobenzene.

Results and Discussion

Synthesis and Characterization. The novel dye-bearing monomers **13**, **14**, **16**, and **17** were synthesized by convergent methods that involved preparing the donor and acceptor portions of the NLO chromophore separately, as illustrated in Schemes I–III. (The general synthetic strategy and the preparation of some of the intermediate compounds have been previously described.[10]) The monomers were isolated as stable crystalline solids, except for compound **17**, which spontaneously polymerized after purification by chromatography, producing an insoluble solid.

The other dye-bearing monomers **13**–**15** were homopolymerized or copolymerized with either methyl methacrylate or with 4-*tert*-butylstyrene to produce NLO-active polymers **1**–**5**, shown in Figure 1. Synthetic data for the polymers are presented in Table I, and characterization data are presented in Table II. The composition of the copolymers **3**–**5** (determined by integration of ^{1}H NMR signals) closely matched the composition of the monomer feed mixture. In addition, comparison of size-exclusion chromatography (SEC) data using differential refractive index detection and using visible absorption detection (at the λ_{max} of the chromophores) demonstrated that the dye-bearing repeat units were distributed uniformly in all molecular weight fractions. These results are consistent with a random sequence distribution for the copolymers,

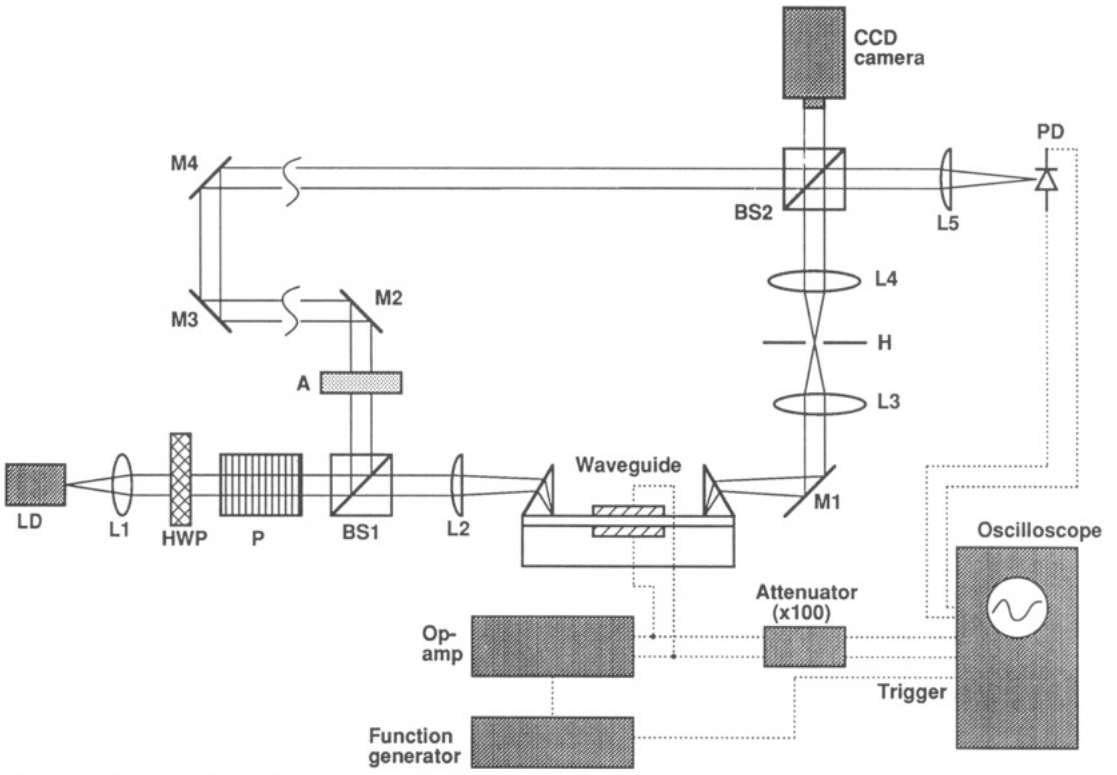

Figure 6. Detailed diagram of experimental setup for Mach–Zehnder interferometry measurements.

Scheme II. Synthesis of Acceptor Portion of NLO Monomers

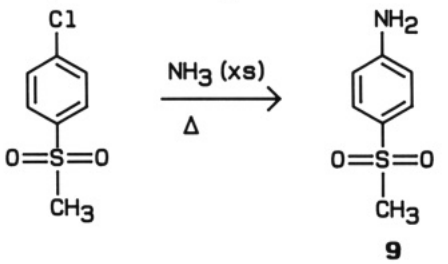

9

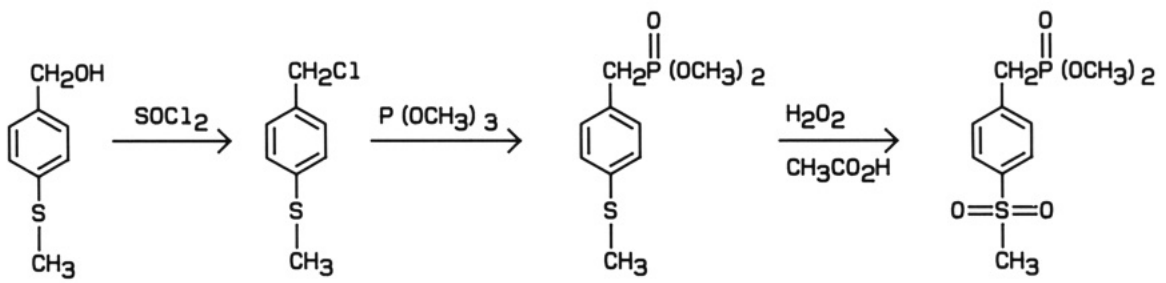

10

in agreement with our earlier data for analogous nitro-containing copolymers.[1]

All of the stilbene compounds were isolated as pure trans isomers, judging from the values of ^{1}H NMR coupling constants of the vinyl protons (~16 Hz). Presumably, the azobenzene compounds were also present in their trans forms, although we do not have any direct evidence for their configuration. The observation of only trans isomers for stilbene and azobenzene derivatives substituted with 4-donor 4′-acceptor groups is consistent with studies of the isomerization of these molecules.[42] The decreased bond order in the central double bond because of the "push–pull" effect allows for facile thermal isomerization to the

Table II. Characterization of NLO Polymers 1–5

polym	$\bar{M}_n$[a]	$\bar{M}_w$[a]	PD[b]	T_g,[c] °C	density,[d] g/cm^3
1	31 400	46 000	1.5	140	[e]
2	38 600	89 000	2.3	99	1.28
3	33 600	92 000	2.7	109	1.20
4	41 100	177 000	4.3	127	[e]
5	25 300	111 000	4.4	109	[e]

[a] Determined by size exclusion chromatography, polystyrene calibration. [b] Polydispersity ($\bar{M}_w/\bar{M}_n$). [c] Determined by differential scanning calorimetry. [d] Measured by helium pychnometry. [e] Not determined. Assumed to be 1.20.

(42) Shin, D.-M.; Whitten, D. G. *J. Am. Chem. Soc.* **1988**, *110*, 5206–5208, and references therein.

Scheme III. Synthesis of NLO Dye Monomers

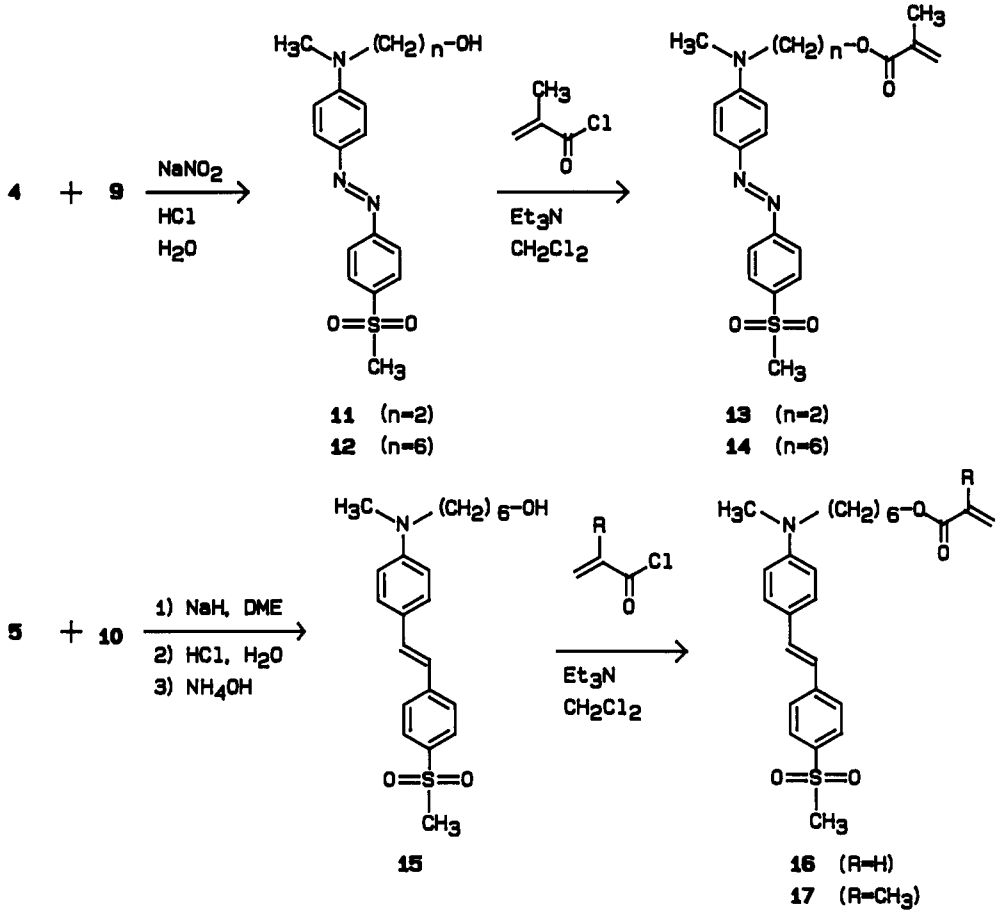

less sterically crowded trans configuration.

As we found earlier with nitrostilbene-containing monomers,[1] polymerization reactions using high concentrations of sulfonylstilbene-containing monomers produced insoluble, cross-linked material. When the concentration sulfonylstilbene-containing monomer was kept low (copolymers 4 and 5), the resulting polymers were soluble but exhibited significant high molecular weight fractions, as detected by SEC. The practical concentration limit of stilbene-containing monomer (before gel formation) is approximately 25 mol %, although we have not thoroughly investigated variations of the reaction conditions. This branching and cross-linking side reaction (apparently through the central double bond of the stilbene unit) is completely absent for polymerizations employing azobenzene-containing monomers. This feature enabled us to synthesize *homopolymers* 1 and 2 that contained more than 60 wt % of NLO-active dye ($>10^{21}$ chromophores cm^{-3}).

Physical Properties. Polymers 1–5 appeared to be amorphous when examined by polarized optical microscopy and by DSC. Glass transition temperatures of 1–5 ranged from 99 to 140 °C (Table II). In contrast, we reported earlier that homopolymers analogous to 2 but containing a nitro group in place of the methylsulfonyl group exhibited crystalline and liquid-crystalline morphologies.[1] The relatively bulky methylsulfonyl group may prevent efficient packing of the aromatic groups and inhibit the formation of an ordered phase.

Because of the amorphous character of the polymers, the order that could be induced by electric field poling was somewhat low (see below), but the optical quality of the materials was excellent. Clear, but highly colored films of polymers 2–5 could be cast from solution onto solid substrates. However, polymer 1 was so brittle (despite its rather high molecular weight) that films tended to crumble and delaminate as the solvent evaporated from the coating. No light scattering caused by crystallites or grain boundaries was present in any of the film samples. In fact, the only detectable scattering from films of these polymers seemed to be caused by dust particles or other macroscopic imperfections. Optical losses were found to be ca. 1 dB/cm at 830 nm for waveguide samples of polymers 2 and 3.

Table III. Linear Optical Data for Polymers 2–4[a]

polym	10^{-20} N[b]	n[c]	λ_{max},[d] nm	OD/[e] μm	ϵ[f]
2	16.8	1.758 (633 nm) 1.662 (860 nm)	446	6.64	4.39
3	7.0	1.623 (633 nm) 1.582 (860 nm)	446	3.50	3.73
4	4.1[g]	1.559 (633 nm)	386	1.46	3.00

[a] Measurements were performed on unpoled polymer samples. [b] Number density of NLO chromophores, determined from ^1H NMR signals and density measurements. [c] Indexes of refraction were determined from waveguiding experiments. [d] Wavelength of maximum absorbance. [e] Optical density per micron at λ_{max}. [f] Dielectric constant measured at 1 kHz and 25 °C. [g] Estimated density of 1.20 g/cm^3 was used to calculate this value.

Optical and Electrical Properties. Table III shows the refractive index, n (measured at 632.8 nm), the wavelength of maximum visible absorption, λ_{max}, the optical density per micron at λ_{max}, and the dielectric constant measured at 1 kHz for unpoled polymer film samples.

Table III clearly shows the effects of dispersion of refractive index for polymers 2 and 3. The relatively high values of n for these two polymers at 632.8 nm occurs because the sulfonylazobenzene chromophore has a slight electronic absorption at this wavelength. Polymer 4, which

has no significant absorption at 632.8 nm, exhibits a refractive index at this wavelength that is more typical of organic materials.

The dielectric constant of all polymers is appreciably higher than n^2, indicating that there is a significant amount of polarization occurring at 1 kHz that cannot respond to an electric field at optical frequencies. This feature may be attributable to small-scale conformational (librational) motions within the glassy matrix.

Prediction of Electrooptic Coefficients. Electric-field-induced second harmonic (EFISH) and standard dipole moment experiments[10] provided the ground-state dipole moment, μ_g, and the second-order hyperpolarizability, β, of the chromophores. A combination of these experiments with ones that determined the linear optical and electrical properties of polymers containing the chromophores allowed the bulk second-order nonlinearity of the materials to be estimated. A comparison of calculated and measured values of the electrooptic coefficient indicates whether poling aligned the dye to the thermodynamic equilibrium or was incomplete for some reason.

The theoretical relationship between molecular hyperpolarizability, β, and the macroscopic susceptibility, $\chi^{(2)}$, of a poled material has been described previously[5,6,9] and is summarized by eq 1, where N is the number density of

$$\chi^{(2)} = N\beta f_0 f_\omega^2 \ell_3\left(\frac{f_0'\mu_g E_p}{kT}\right) \quad (1)$$

NLO molecules, f_0 and f_ω are local field factors, ℓ_3 is the Langevin function describing the orientation, μ_g is the ground-state dipole moment, and E_p is the poling electric field.

The Lorenz–Lorentz field factor f_ω, which relates the local optical field of the material to the external optical field, is given by

$$f_\omega = (n_\omega^2 + 2)/3 \quad (2)$$

where n_ω is the index of refraction at frequency ω. The Onsager field factor, f_0, which relates the local electric field to the applied electric field, is given by

$$f_0 = \frac{\epsilon_0(n_\infty^2 + 2)}{(n_\infty^2 + 2\epsilon_0)} \quad (3)$$

where n_∞ is the index of refraction at optical frequencies and ϵ_0 is the dielectric constant. For f_0 in eq 1, ϵ_0 is measured at the conditions of the electrooptic experiment, while for f_0', ϵ_0 is measured at poling conditions.

In the calculation of electrooptic coefficients, we used measured values of β and μ_g.[10] It should be pointed out that these values can be calculated based on the molecular structure of the chromophore using molecular mechanics. In our experience, the dipole moments are calculated accurately, but hyperpolarizability values are usually underestimated, possibly because the β calculation applies to isolated molecules and ignores interactions that may be present in the bulk.

The hyperpolarizability for second-harmonic generation, $\beta(-2\omega';\omega',\omega')$, was determined from EFISH experiments at 1.9 μm.[10] The corresponding hyperpolarizability for electrooptics, $\beta(-\omega;0,\omega)$, was estimated from $\beta(-2\omega';\omega',\omega')$ according to a two-level model of the electronic levels of the dye using

$$\frac{\beta(-\omega;0,\omega)}{\beta(-2\omega';\omega',\omega')} = \frac{(3\omega_0^2 - \omega^2)(\omega_0^2 - \omega'^2)(\omega_0^2 - 4\omega'^2)}{3\omega_0^2(\omega_0^2 - \omega^2)} \quad (4)$$

where ω_0 is the angular frequency of absorption of the first excited state.

Table IV. Nonlinear Optical Data for Polymers 2–4 Measured by Ellipsometry at 632.8 nm

polym	V_p,[a] V/μm	T_p,[b] °C	dΔ/dV,[c] rad/V	r_{33}(exp),[d] pm/V	r_{33}(calcd),[d] pm/V
2	137	100	47.1	38.7	29.8
3	89	120	15.1	12.9	7.8
4	181	120	2.9	2.6	6.8

[a] Electric field during poling. [b] Temperature during poling. [c] Change in ellipsometric constant with voltage. [d] Electrooptic coefficient.

The magnitude of the electrooptic effect in a material is normally expressed in terms of the electrooptic coefficient, r, which is related to the electric-field-induced change in refractive index by

$$\Delta\frac{1}{n_{ij}^2} = r_{ijk}E_k \quad (5)$$

The first two subscripts of r are customarily contracted because n_{ij} has the symmetry $n_{ij} = n_{ji}$. The electrooptic coefficient in meters per volt is related to $\chi^{(2)}$ in esu by

$$r_{33} = \frac{8\pi}{3 \times 10^4 n^4}\chi^{(2)}_{zzz}(-\omega;0,\omega) \quad (6)$$

Electrooptic Measurements at 632.8 nm by Ellipsometry. We measured the values of r_{33} for poled film samples polymers **2–4** by observing with an ellipsometer the relative phase shift, Δ, of a HeNe laser beam passed through the sample as a function of applied voltage across the sample. Δ was found to vary linearly with V. The electrooptic coefficient of the polymer was calculated from the slope dΔ/dV using the equation[40,41]

$$d\Delta/dV = \tfrac{2}{3}kn^3 \tan\phi \sin\phi\, r_{33} \quad (7)$$

where k is the wavenumber of the light beam in air, ϕ is the propagation angle of the beam in the polymer with respect to the film normal, and r_{33} is the element of the electrooptic tensor pertaining to normal components of the induced refractive index change along the applied electric field. Table IV shows the poling conditions along with the calculated and measured electrooptic coefficient of three polymer films at 632.8 nm.

In the calculation of r_{33} we used n at 632.8 nm, and ϵ at 1 kHz and 25 °C in both the Lorenz–Lorentz and Onsager field factors. The ground-state dipole moment, μ_g, and the molecular hyperpolarizability, β, for the appropriate dye were taken from ref 10.

The calculated and experimental electrooptic coefficients here agree within a factor of about 2. There are several potential sources for this discrepancy. The calculated r_{33} is based on contributions only from electronic polarization, whereas the experimental r_{33} may include additional contributions from vibrational and conformational polarizations. Also, since r_{33} was measured with dc voltage, it is possible that electrostriction and third-order NLO effects may contribute to its apparent value. However, the above contributions to r appear to be negligible in this case because the electrooptic effect was absent in unpoled films and was found to be a linear function of the applied voltage in poled films. A more significant error may be introduced because the value of ϵ used in the Onsager field factor f_0' should be determined at the poling temperature at extremely low frequency. However, these conditions are experimentally inaccessible, and we used values for ϵ measured at 25 °C and 1 kHz. This substitution results in a field factor f_0, which is too low. The largest source of error in calculating r_{33} probably is caused by the dispersion correction using the two-level model (eq 4). It is

known that higher excited states contribute significantly to the hyperpolarizability. The accuracy of r_{33} predictions is much improved for longer wavelengths (see below) at which the dispersion correction is smaller.

It should also be pointed out that EFISH measurements on the chromophores were performed in solution, and it is unknown how $\mu\beta$ values translate from solution to the solid state. However, in light of the reasonable agreement between predicted and measured electrooptic coefficients, the solution measurements probably give reliable values.

While the electrooptic coefficients measured for polymers **2**–**4** as listed in Table IV compare favorably with the most common inorganic NLO material, lithium niobate (r_{33} = 32 pm/V), we emphasize that the coefficients for azobenzene-containing polymers **2** and **3** are resonance enhanced because of slight absorbance at 632 nm (the wavelength of the HeNe laser used in testing), and their nonresonant r_{33} values are lower (see below).

Electrooptical Properties in the Near-Infrared Measured by Mach–Zehnder Waveguide Interferometry. This technique involves the measurement of the electrooptically induced phase shift in a NLO waveguide that has been incorporated in the sample arm of a Mach–Zehnder interferometer. This prototypical device provides another means for determining the linear electrooptic coefficients for poled NLO polymer films, in this case in a wavelength region that is important for many optical devices.

Planar optical waveguides are formed by multiple transparent dielectric layers that are arranged so that the inner layers (core region) have *higher* effective refractive indexes than do the outer layers (cladding regions). Light propagating in the core region is trapped in this region provided that the angles of incidence at both core-cladding interfaces exceed the critical angles at these interfaces. If the thickness of the core region approximates the wavelength of light, only one or two allowable propagating modes may exist.[43] Transverse magnetic (TM) modes are those in which the magnetic field vector of the propagating light is in the film plane and transverse electric (TE) modes are those in which the electric field vector is in the film plane. If the optical absorption losses in the various layers are low enough, waveguide structures provide ideal means for accurate determination of relatively weak effects such as the linear electrooptic effect. This is true for two reasons: the confinement of light to the core region results in an efficient overlap between the externally applied dc electric field and the optical field, and the relatively long pathlengths available increase the phase shift for a given induced electrooptically induced change in refractive index.

An additional advantage in using waveguides to measure electrooptic coefficients is that both r_{33} and r_{13} are accessible through measurement of the phase shifts induced in the TM and TE modes, respectively. Arguments based on symmetry considerations require that $r_{13} = r_{23}$ and $r_{33} = 3r_{13}$ for poled glassy polymers because of their symmetry class $C_{\infty v}$.[2] The ellipsometric measurements of r_{33} described in the previous section implicitly assume that the stated relationship to r_{13} holds.[44]

Figure 2 is a cross-sectional schematic of the waveguide structure used in these experiments. Also defined in this figure is the coordinate system used in the analysis. Fabrication of waveguide samples is discussed in more detail in the Experimental Section. The waveguide core was formed from a thin film of NLO polymer, the upper cladding layer was an indane derivate monomer glass,[45] and the substrate (lower cladding) was soda lime glass. The upper cladding also served as a buffer between the upper gold electrode and the waveguide core. No buffer was used between the NLO core and the lower indium tin oxide (ITO) electrode. Fields in the electrooptic measurements were applied by means of the electrodes positioned above and below the NLO core. Prisms were used to couple light into and out of the NLO film in regions where the gold electrode was absent.

As mentioned in connection with eq 5, electrooptically induced refractive index changes in bulk samples are proportional to the linear electrooptic coefficients, r_{ij}. Using the coordinate system convention in Figure 2 and assuming that the electric field is applied only along the $\hat{z}$ axis, eq 5 can be rewritten as

$$\Delta\frac{1}{n_{33}^2} = -2n_f^{-3}\Delta n_{33} = r_{33}E_3 \tag{8}$$

or

$$\Delta n_{33} = -(n_f^3/2)r_{33}E_3 \tag{9}$$

where Δn_{33} is the index change for light polarized along the $\hat{z}$ axis due to the applied field E_3 along the $\hat{z}$ axis. n_f is the index of refraction of the isotropic (unpoled) NLO polymer. A similar expression can be written for Δn_{13}:

$$\Delta n_{13} = -(n_f^3/2)r_{13}E_3 \tag{10}$$

Δn_{13} is the index change along the $\hat{x}$ axis due to the electric field along the $\hat{z}$ axis.

It can be shown through simple perturbation analysis that the relationship corresponding to eqs 9 and 10 for guided modes have the forms

$$\Delta n_{\text{eff,TMm}} \approx -\gamma_{\text{TMm}}(n_f^3/2)r_{33}E_3 \tag{11}$$

$$\Delta n_{\text{eff,TEm}} = -\gamma_{\text{TEm}}(n_f^3/2)r_{13}E_3 \tag{12}$$

where $\Delta n_{\text{eff,TMm}}$ and $\Delta n_{\text{eff,TEm}}$ are the changes in the *effective* indexes for mth-order TM and TE modes, respectively, and

$$\lambda_{\text{Nm}} = \int_0^{t_f}|F_{\text{Nm}}(z)|^2\,dz \Big/ \int_{-\infty}^{+\infty}|F_{\text{Nm}}(z)|^2\,dz \tag{13}$$

is the overlap integral of the applied electric field and the square of the magnitude of the optical field. In this equation, t_f is the thickness of the NLO polymer film. $F_{\text{Nm}}(z)$ represents for the mth-order mode the transverse electric field distribution for N = TE and represents the transverse magnetic field distribution for N = TM. In deriving eq 13, it was assumed that the applied electric field is uniform throughout the NLO polymer film and that the NLO polymer layer is the only layer that exhibits the linear electrooptic effect. Equation 13 also assumes that the optical anisotropy of the waveguide can be ignored, that the electrooptically induced index change is much smaller than n_f, and that the effective index of the guided mode is approximately equal to n_f. Equation 11 shows the $\approx$ sign to emphasize that this analysis has ignored the small components of the electric field vector of the TM mode along the $\hat{x}$ axis. Strictly speaking, $\Delta n_{\text{eff,TMm}}$ should include contributions from both r_{13} as well as r_{33}. In cases where the TM mode is far from the cutoff, the error introduced

(43) See for example: Kogelnik, H. In *Topics in Applied Physics: Integrated Optics*; Tamir, T., Ed.; Springer-Verlag: Berlin, 1979; Topics in Applied Physics, Vol. 7; Chapter 2.

(44) Note that control experiments using second harmonic generation performed on poled samples of the polymers in this study independently confirmed that $r_{33} = 3r_{13}$.

(45) Scozzafava, M.; Dao, P. T.; Robello, D. R.; Schildkraut, J. S.; Willand, C. S.; Williams, D. J. U.S. Patent 4,946,235, 1990.

Table V. Physical Parameters for Mach–Zehnder Waveguide Samples

sample	t_f,[a] μm	t_c,[b] μm	γ_{M0}[c]	L, mm
2A	1.72	2.00	0.99	8.02
2B	2.00	2.00	0.99	6.00
2C	2.00	2.00	0.99	4.00
3A	2.30	3.00	0.97	6.35
3B	2.30	3.00	0.97	8.60

[a] Thickness of the NLO polymer layer. [b] Thickness of the upper buffer layer. Note that the index of refraction of the monomer glass used for this buffer layer was 1.54, determined from waveguiding experiments. The index of refraction of soda lime glass (used as substrate) was estimated to be 1.51 from visible index and dispersion data. [c] $\gamma_{TE0} \approx \gamma_{TM0}$ in all samples.

by this simplification is not significant.

The electric field applied to the NLO polymer film can be calculated from the applied voltage, the thicknesses of the NLO polymer and monomer glass cladding films, and the dc dielectric constants of these films. Referring to Figure 2 and applying the usual formula for capacitive voltage division, one obtains

$$E_3 = V_3/t_f = \epsilon_c V/(\epsilon_f t_c + \epsilon_c t_f) \quad (14)$$

where V is the externally applied voltage and V_3 is the voltage across the NLO film. ϵ_f, ϵ_c, t_f, and t_c are the dielectric constants and thicknesses, respectively, of the NLO polymer and monomer glass cladding layers.

Figure 3 is a schematic representation of a Mach–Zehnder interferometer. Light from a laser diode LD is split into two branches by beamsplitter BS1. The light in one of the branches is coupled into the waveguide sample and experiences a phase shift given by

$$\Phi_s(V) = k\Delta n_{eff,Nm}(V)L + \Phi_{s,o} \quad (15)$$

where $k = 2\pi/\lambda$, λ is the wavelength of light in vacuum, and L is the electrode length along the propagation direction. $\Phi_{s,o}$ is the portion of the phase shift in the sample arm of the interferometer, which is independent of applied field. Light in the other branch serves as reference and has phase shift $\Phi_{r,o}$. When the sample and reference beams are recombined at beamsplitter BS2 they interfere. The light intensity measured at the photodetector is given by

$$I(V) = I_0 \cos^2 [\Delta\Phi(V)/2] \quad (16)$$

assuming that the intensities of light in the reference and sample arms are equal. I_0 is the intensity maximum and $\Delta\Phi(V) = \Phi_s(V) - \Phi_{r,o}$. It can be seen from eq 16 that a change in voltage that generates a phase shift of $\Delta\Phi = \pi$ (corresponding to one half-wave of retardation) will cause the intensity to go from a maximum to a minimum. Referring to this voltage as V_π and combining eqs 11, 12, 14, and 15, one can obtain a relationship between V_π and the electrooptic coefficients:

$$r_{ij} = \frac{\lambda}{n_f^3} \frac{(\epsilon_f t_c + \epsilon_c t_f)}{V_{\pi,Nm}\epsilon_c \gamma_{Nm} L} \quad (17)$$

Equation 17 permits determination of r_{ij} from measured values of the half-wave voltage, $V_{\pi,Nm}$, as well as other quantities appearing on the right hand side of this equation.

Figure 4 shows an oscilloscope trace for a typical Mach–Zehnder interferometer experiment. In this example infrared light (λ = 860 nm) was coupled into the TM0 mode of a waveguide formed of NLO polymer **3** (sample A). Superimposed on the trace are the photodetector output and applied input voltage. The voltage was ramped linearly in time from 0 to 160 V. As can be seen, the light intensity varies sinusoidally in time in accordance with the predictions of eqs 15 and 16. From this data, the half-wave voltage is determined to be about 31 V. Substituting this value of $V_{\pi,TM0}$ into eq 17 along with values of the dielectric constants, film thicknesses, overlap integrals, and electrode lengths from Tables III and V, a value of r_{33} = 6.28 pm/V is obtained. (Note: a value of ϵ_c = 3.5 was measured for the dielectric constant of the monomer glass.) The overlap integrals, γ_{TM0} and γ_{TE0}, were determined from the calculated m = 0 mode field distribution profiles using the indexes of refraction and the thicknesses tabulated in Table V.

Table VI summarizes experimental and theoretical values obtained for r_{ij} in the infrared for selected NLO polymer samples. These results represent measurements taken on freshly poled (i.e., within days of poling) samples of NLO polymers **2** and **3** and show the effects of poling field magnitude and mode polarization on the electrooptic coefficients. As can be seen, better agreement is obtained between theory and experiment for samples **3A**, **3B**, and **2A** in the infrared than was obtained for these polymers by ellipsometry at 632.8 nm (previous section). On the other hand, the agreement between theory and data is about the same for samples **2B** and **2C** at infrared and visible wavelengths. The lack of agreement for samples **2A** and **2C** in the infrared may be due to uncertainties associated with the measurement of the poling field for these samples.

r_{13} coefficients were measured only for polymer **3**. Experimental values for the ratio r_{33}/r_{13} are found to be 3.09 and 3.11 for samples **3A** and **3B**, respectively, in good agreement with theory, which predicts a ratio of 3.

Measurements made on samples of polymer **3** over a period of nearly 2 years (during which time the samples were stored under ambient conditions) demonstrated that the electrooptic coefficient fell to approximately 50% of its initial value during the first 6 months, then stabilized.

We also found that measured values of r_{33} depended on the polarity of the Au electrode with respect to the ITO electrode. For example, the electrooptic coefficient for sample **3** (after 730 days) obtained with Au positive with respect to ITO was r_{33} = 3.22 pm/V, whereas a value of r_{33} = 2.87 pm/V was obtained when the polarities of the electrodes were reversed. This represents about 12% of the total electrooptic coefficient. (No special care was taken to observe the electrode polarity prior to t = 730

Table VI. Nonlinear Optical Data Measured in the Near-Infrared Region by Mach–Zehnder Waveguide Interferometry for Polymers 2 and 3

sample	E_p,[a] (V/μm)	$V_{\pi,TM0}$,[b] V	$V_{\pi,TE0}$,[b] V	r_{33}(exp), pm/V	r_{33}(calcd) pm/V	r_{13}(exp),[c] pm/V	r_{13}(calcd), pm/V
2A[d]	99	7.61 ± 0.03	*f*	12.53 ± 0.05	11.86	*f*	3.95
2B[d]	~70	12.50 ± 0.07	*f*	10.90 ± 0.06	8.40	*f*	2.80
2C[d]	~70	17.2 ± 0.5	*f*	11.9 ± 0.4	8.40	*f*	2.80
3A[e]	100	31.2 ± 0.3	96 ± 3	6.24 ± 0.06	5.40	2.0 ± 0.1	1.80
3B[e]	86	30.6 ± 0.6	95 ± 3	4.69 ± 0.10	4.64	1.5 ± 0.1	1.55

[a] Voltage applied during poling. Note that the poling temperatures for all samples was between 89 and 90 °C. [b] Voltage required for a π phase shift (see text). [c] Electrooptic coefficient. [d] Measurements made at 860 nm. [e] Measurements made at 830 nm. [f] Not determined.

days.) It is not known exactly why these measurements should be polarity dependent; however, the correct explanation probably has to do with the built-in asymmetry in the waveguide/electrode structure. One possible explanation is that the ITO/NLO interface is acting primarily as a hole injector.[46] If this is true, space charge buildup in the NLO film would be more pronounced with the ITO electrode positive than with the ITO electrode negative. This would result in a smaller average electric field inside the NLO film and a lower apparent electrooptic coefficient for ITO positive. An alternative explanation is that a larger space charge built up in the monomer glass because hole mobility is much larger than electron mobility in this layer.[47] A larger space charge in the monomer glass buffer would force a larger field across the NLO film and would result in a larger apparent electrooptic coefficient. Indeed, any combination of these two effects (i.e., hole injection into the NLO or into the monomer glass buffer) could explain the observed polarity dependence.

Conclusions

We have successfully synthesized polymers bearing pendant chromophores with strong NLO activity. The moderately large electrooptic coefficients measured for poled samples of these polymers could be predicted with reasonable accuracy based on measurements of molecular properties (μ_g and β) and linear optical properties of the materials. However, because of assumptions and uncertainties inherent to the calculations, discrepancies between predicted and experimental values of r_{33} cannot be attributed solely to nonelectronic contributions. Prototype electrooptic devices have been constructed, but it is clear that stronger chromophores and improved stability of alignment will be required for any practical applications. Studies directed to address these issues and to investigate the dynamics of the orientation of these polymers are in progress and will be reported later.

Acknowledgment. We express our appreciation to M. Thomas and J. Reiff for SEC measurements, to V. Mazzio and M. Moscato for DSC measurements, and to S. B. Crayton and E. J. Voll for density measurements, all members of Eastman Kodak Analytical Technology Division. We acknowledge J. O'Reilly for DSC measurements on polymer 1, and E. Prince for preparing the ITO layers used in waveguiding experiments, both of Eastman Kodak Corporate Research Laboratories. We also thank C. A. Maggulli, M. Lodollini, and D. White of the GLM Telesis Co. for synthetic assistance.

Registry No. 1 (homopolymer), 139278-65-2; 2 (homopolymer), 139278-66-3; 3 (copolymer), 139278-67-4; 4 (copolymer), 139278-68-5; 5 (copolymer), 139278-69-6; 6, 122-98-5; 7, 93-90-3; 8, 120654-22-0; 9, 5470-49-5; 10, 139278-57-2; 11, 139278-55-0; 12, 139278-56-1; 13, 139278-59-4; 14, 139278-60-7; 15, 139278-58-3; 16, 139278-61-8; acryloyl chloride, 814-68-6.

(46) Tang, C. W.; VanSlyke, S. A. *Appl. Phys. Lett.* **1987**, *51*, 913.
(47) Stolka, M.; Yanus, J. F.; Pai, D. M. *J. Phys. Chem.* **1984**, *88*, 4707.

Structure and Properties of the Transition-Metal Zintl Compounds: $A_{14}MnBi_{11}$ (A = Ca, Sr, Ba)

Traci Y. Kuromoto,[†] Susan M. Kauzlarich,*[,†] and David J. Webb*[,‡]

Departments of Chemistry and Physics, University of California, Davis, California 95616

Received October 10, 1991. Revised Manuscript Received December 9, 1991

$A_{14}MnBi_{11}$ (A = Ca, Sr, Ba) is synthesized by reacting the elements in stoichiometric amounts at high temperatures (950–1350 °C). Single-crystal X-ray diffraction data (130 K, a = 17.002 (6) Å, c = 22.422 (7) Å (Ca); a = 17.820 (6) Å, c = 23.394 (6) Å (Sr); a = 18.633 (8) Å, c = 24.340 (10) Å (Ba)) were refined (tetragonal, $I4_1/acd(142)$, Z = 8, R = 5.4%, R_w = 5.9% (Ca), R = 4.1%, R_w = 4.7% (Sr), R = 5.1%, R_w = 4.9% (Ba)) and showed these compounds to be isostructural to the main-group analogues, $Ca_{14}AlSb_{11}$ and $A_{14}GaAs_{11}$ (A = Ca, Sr). Magnetization measurements performed on powder samples have shown that $Ca_{14}MnBi_{11}$ and $Sr_{14}MnBi_{11}$ are ferromagnets and that $Ba_{14}MnBi_{11}$ is an antiferromagnet. The magnetic coupling between Mn ions is attributed to an RKKY interaction, and thus metallic behavior is expected. The temperature dependence of the resistivity of pressed pellets is presented and suggests that all three compounds are metals.

Introduction

Many bonding schemes have been suggested for the wide variety of materials that exist. These vary from the Hume-Rothery[1] rules for intermetallic compounds to the simple valence rules for insulating compounds.[2] There are a large number of solid-state compounds whose structures can be understood by a simple electron-counting scheme referred to as the Zintl concept.[3,4] The initial suggestions of E. Zintl concerned binary compounds composed of an alkali or alkaline earth metal and a main-group element. Zintl proposed that the structures and properties of these phases could be understood by considering the compound to be composed of an electropositive metal which transfers its electrons to the electronegative element which in turn forms the correct number of homoatomic bonds such that each element has a complete octet.[5] The

[†] Department of Chemistry.
[‡] Department of Physics.
* To whom correspondence should be addressed.

(1) Hume-Rothery, W. *J. Inst. Met.* **1926**, *35*, 313.
(2) Pauling, L. *The Nature of the Chemical Bond*, 3rd ed.; Cornell University Press: Cornell University, 1960.
(3) (a) Schäfer, H.; Eisenmann; B.; Müller, W. *Angew. Chem., Int. Engl.* **1973**, *12*, 694, (b) Schäfer, H.; Eisenmann, B. *Rev. Inorg. Chem.* **1981**, *3*, 29, (c) Schäfer, H. *Annu. Rev. Mater, Sci.* **1985**, *15*, 1, (d) Schäfer, H. *J. Solid State Chem.* **1985**, *57*, 97.
(4) Nesper, R. *Prog. Solid State Chem.* **1990**, *20*, 1.
(5) Zintl, E. *Angew. Chem.* **1939**, *52*, 1.

0897-4756/92/2804-0435$03.00/0